Nylon 6 Crystal Structures, Folds, and Lamellae from Theory

Youyong Li and William A. Goddard III*

Materials and Process Simulation Center (Mail Code 139-74), Division of Chemistry and Chemical Engineering, California Institute of Technology, Pasadena, California 91125

Received May 28, 2002; Revised Manuscript Received July 24, 2002

ABSTRACT: Although polyamide "nylon 6" polymer is an important industrial material, there remain many questions about the details of the various structures and the conversion between them. Using the MSXX force field (developed previously from ab initio quantum calculations), we predict the crystal structures, folds, and lamellae of nylon 6, leading to the following results. (a) Assuming infinite chains and evaluating the free energy of all 112 regular crystal structures, we find three classes of crystal structures: α form, γ form, and δ form. We find that at 300 K the α form is most stable, with γ and δ higher by 0.4 and 0.3 (kcal/mol)/(amide unit), respectively. We calculate Young's modulus in the chain direction to be 295 GPa for α, 135 GPa for γ, and 253 GPa for δ. These values are above the experimental value of 168 GPa for α form because the experimental system has a finite lamella thickness, disorder in the chain conformation, and imperfections in the crystallinity. (b) We find the thermostability of α form over other forms arises from *intra-H-bonds* in the α form, which are dynamically and entropically favored. (c) We propose five detailed steps in the transition between the α and γ forms. We also identify the structures of the other two experimentally observed metastable forms, β and δ. Our structures explain the available fiber X-ray results. (d) The H-bond schemes for all regular crystal structures are examined. We find that the γ form has a more linear (stronger) H-bond than α form, which is consistent with the interpretation from solid-state NMR. (e) Considering that nylon forms lamellae with finite thickness in the chain direction we considered all five possible loop structures and the two best (of eight) possible stacking schemes for the folded sheets together with the 14 possible sheet displacements. We find that the optimum lamella for α form has the alkane loop fold (one amide per loop) and packs so that adjacent sheets are displaced by ± 3.7 Å (3*b*/14), which is in good agreement with the conclusion from fiber X-ray. Our amide pocket model explains the observed sheet displacements in nylon 6 and nylon 66 and also the progressive shear in nylon 66 and nylon 46.

1. Introduction

The polyamide "nylon 6" polymer is an important polymeric material with applications ranging from carpet and automotive parts to intimate apparel.[1] In addition, nylon 6 stores a larger amount of iodine[2] than any other polymer, and it is claimed to be a good solid-state electrolyte.[2] Nylon 6 has the [−NH(CH$_2$)$_5$(CO)−] repeating group, leading to a structure in which the peptide units (NH−CO) provide hydrogen bonding between polymer chains. Although nylon is highly crystalline, the presence of the crystalline lamella in an amorphous matrix makes it difficult to obtain precise crystallography. Despite the numerous important industrial applications and numerous experimental studies on nylon 6, there remain many questions about the details of the various structures and the conversion between them. As with other highly crystalline polymers (such as polyethylene and PET), the chains in the crystalline regions of nylon 6 tend to be re-entrant to preserve chain−chain bonding, and the nature of these folds complicates the optimum spacing and structure of the lamella and the connections between them.

To learn about the various factors controlling these structures and their properties, we used the MSXX force field developed by Dasgupta et al.[3] to carry out theoretical calculations (quantum mechanics, molecular dynamics, and molecular mechanics) to determine the optimum packing and fold structures of nylon 6. Section 2 describes the details of these methods. Section 3 reports the results for infinite chain model structures of nylon 6 and compares to the experimental data. Section 4 discusses the results for fold structures of nylon 6. The summary is in section 5.

* To whom correspondence should be sent: E-mail: wag@wag.caltech.edu.

2. Calculation Details

We used the MSXX FF[3] with the MSC version of PolyGraf (version 3.30, Caltech version) for all calculations. Some quantum mechanics (QM) simulations were performed to validate the results with the MSXX FF. Cerius2 (v4.0) was also used for graphics and manipulations. The electrostatic and van der Waals (vdW) interactions used the accuracy-bounded convergence acceleration (ABCA) Ewald technique[4] for computing the nonbond energies of periodic systems. We used an accuracy of 0.001 kcal/mol. All structures were minimized to an rms force on all atoms of 0.01 kcal/(mol Å) for atom and rms stresses of 0.1 kcal/(mol Å) using conjugate gradient method.

2.1. Force Field. The MSXX force field for simulation of nylon polymers was derived from ab initio QM calculations.[3] Special emphasis was given to the accuracy of the hydrogen bond potential for the amide unit and the torsional potential between the peptide and alkane fragments.

This hydrogen bond potential was derived from MP2/6-31G** calculations of the formamide dimer. Subtracting electrostatic interactions (based on fixed-point charges extracted from QC on the monomers) leads to a repulsive exponential form (eq 1) of the short-range hydrogen bond potential[3] with $A = 0.028$ kcal/mol, $C = 0.251$ Å, and $R_e = 3.017$ Å. Instead of the original charge scheme in ref 3, we now use the improved charge scheme from

10.1021/ma020815n CCC: $22.00
Published on Web 09/27/2002

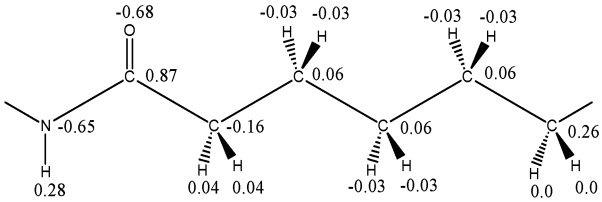

Figure 1. Charge scheme for a monomer fragment in polymer chain of nylon 6.

ref 5 (see section 2.2). The differences are mainly from the methylene groups, which do not affect the parameters used for hydrogen bond potential.

$$E_{\mathrm{vdW}}^{\mathrm{EXP}} = A \exp\left[-\frac{(R - R_{\mathrm{e}})}{C}\right] \tag{1}$$

The full torsion potential between peptide and alkane fragment was calculated by optimizing the geometry (using HF/6-31G**) at each point on the torsional curve and the torsional potential is represented by a Fourier series (eq 2) in MSXX force field.[3]

$$E_{\mathrm{torsion}} = \frac{1}{2}\sum_{n=0}^{n=6} V_{\mathrm{n}} \cos n\tau \tag{2}$$

where τ is the torsional angle ($\tau = 0$ for cis) and V_{n} is the barrier (energy of cis over trans).

The detailed MSXX force field was described in a previous paper.[3]

2.2. Charges. We use potential derived charges (PDQ) based on quantum mechanical calculations (HF/6-31G**) of model systems. These charges are based on calculations for long alkyl chains functionalized with an amide linkage, where a minimum of five carbons to either side was required for charge convergence.[5] On the basis of a series of calculations for shorter alkane chains functionalized with an amide, the charge perturbation within a long alkane chain due to each functional unit was extracted.[5] The charge scheme for nylon 6 is summarized in Figure 1.

2.3. Vibrational Calculations. The analytic second derivative matrix (Hessian) obtained directly from the complete energy expression was used to calculate the vibrational modes and frequencies. This Hessian was also used with additional terms to calculate the elastic constants (including Young's modulus). To obtain the zero point energy and temperature-dependent entropy (S), enthalpy (H), and free energy (F) as a function of temperature, we calculated the vibrational modes for a $3 \times 3 \times 3$ mesh of reciprocal lattice vectors, based on the unit cell with four chains each with two formula units. We also used a $5 \times 5 \times 5$ mesh for the model structure proposed by Holmes[6] and found a total free energy change of only 0.03 (kcal/mol)/(amide unit). The methodologies are reported in ref 7, 8 and implemented in the VIBRATE, THERMO, and ELASTICA Modules in PolyGraf.

2.4. *R*-Factor Calculation. We used the "Diffraction-Crystal" module in Cerius2 4.0 to calculate the fiber X-ray diffraction intensities and to obtain the R-factor against the experimental data. The intensity for each hkl reflection was calculated using

$$I(hkl) = \{\sum f_n \cos 2\pi(hx_n + ky_n + lz_n)\}^2 + \{\sum f_n \sin 2\pi(hx_n + ky_n + lz_n)\}^2 \tag{3}$$

where f_n is the scattering factor of atom n and x_n, y_n, z_n are the fractional coordinates of atom n. The summation is over all atoms in the unit cell.

We used the global anisotropic temperature factor to correct the intensities. In this method, the intensity of an hkl reflection is reduced by a factor of the form

$$\exp[-2(h^2B_a + k^2B_b + l^2B_c)] \tag{4}$$

where $B_a = 2\pi^2\langle a^2\rangle/a^2$, $B_b = 2\pi^2\langle b^2\rangle/b^2$, and $B_c = 2\pi^2\langle c^2\rangle/c^2$ are dimensionless. $\langle a^2\rangle$, $\langle b^2\rangle$, and $\langle c^2\rangle$ are mean squared atomic displacements (Å^2) in a crystal with unit cell dimensions a, b, c (Å). We determined the $\langle a^2\rangle$, $\langle b^2\rangle$, and $\langle c^2\rangle$ from NVT molecular dynamics simulations.

No polarization factor or crystal monochromator factors were applied to the intensity calculation.

The R-factor is defined as follows:

$$R = \frac{\sum |I_{\mathrm{obsd}} - I_{\mathrm{calcd}}|}{\sum I_{\mathrm{obsd}}} \tag{5}$$

3. Infinite Chain Model Structures of Nylon 6: Results and Discussion

3.1. α Form, γ Form, and Intermediate Forms from Fiber X-ray Experimental Results. Two crystalline forms in nylon 6, α and γ, have been well characterized by X-ray crystallography.[6,9,25−27] The plane of the amide group and that of the $(CH_2)_5$ group are parallel in the α form, while in the γ form they are approximately perpendicular. H-bonds are formed between antiparallel full-extended chains in the α form and between parallel pleated chains in the γ form. The α phase is the thermodynamically most stable crystalline form, and can be obtained by slow cooling from the melt. The γ form is obtained by spinning fibers at a high speed or by iodinating nylon 6 in aqueous KI/I_2 treatment followed by removal of the iodine and potassium with sodium thiosulfate. The γ form can be converted into α by melting followed by recrystallization,[10] by annealing at 160 °C in a saturated-steam atmosphere without any significant loss of orientation,[11] and by applying stress at room temperatures.[12−14]

Besides the well-characterized α form and γ form, there exists the intermediate crystalline phases between them,[15−24] which we will discuss in part 3.5.

3.2. All Possible Regular Infinite Chain Crystal Structures of Nylon 6. There are two distinct different chain conformations of nylon 6: full-extended chain and twisted chain as shown in Figure 2. H-bonds can be formed between antiparallel chains or parallel chains. The corresponding chains in adjacent sheets can be antiparallel or parallel. Thus, there are four possible packing schemes of the chains.

From the two types of chain conformations and the four packing schemes, eight possible classes of regular infinite chain crystal structures are constructed as shown in Figure 2.

We will classify the structures using a 3-letter index:

1. The first letter describes whether the chains are full-extended (E) or twisted (T).

2. The second letter describes the relative direction of the chains *forming H-bonds* parallel (P) or antiparallel (A).

3. The third letter describes the relative direction of corresponding chains in *adjacent sheets* parallel (P) or antiparallel (A).

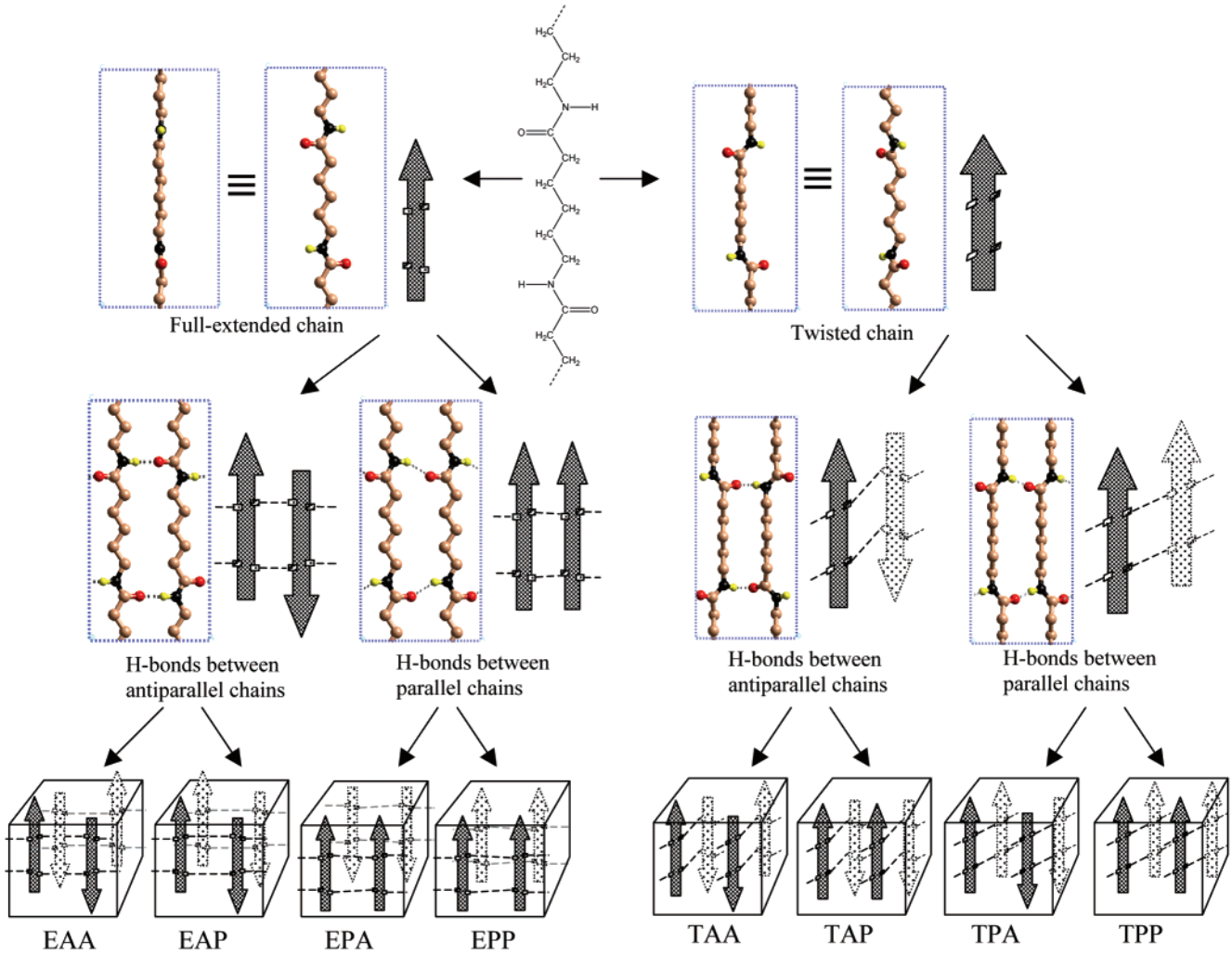

Figure 2. Eight possible classes of crystal structures constructed with different packing schemes.

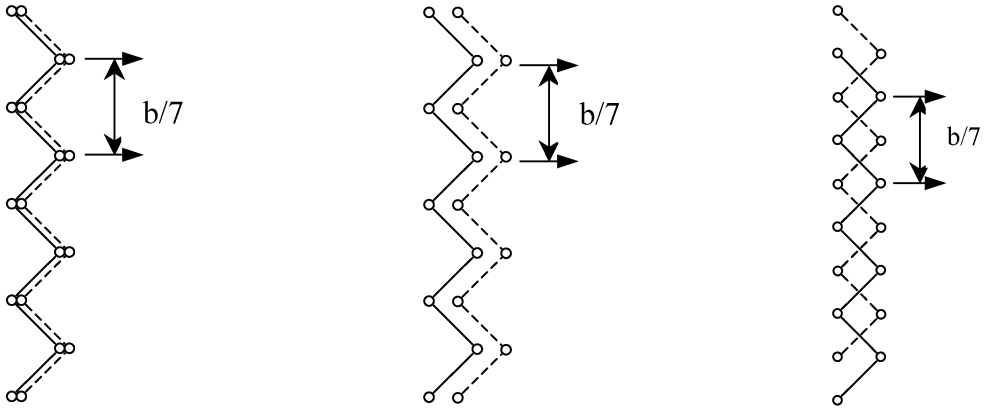

a. *"uncrossed"-chains* b. *shift "uncrossed"-chains* c. *"crossed"-chains*

Figure 3. Three stacking schemes of polymer chains in adjacent sheets.

The eight classes of crystal structures EPP, EPA, EAP, EAA, TPP, TPA, TAP, and TAA are shown in Figure 2.

There are three distinct ways to stack adjacent H-bond sheets in nylon 6 crystal, as illustrated in Figure 3. The two chains shown in parts a−c represent the corresponding chains in adjacent H-bond sheets. In Figure 3b, the two chains are shifted in both *b* and *a* directions (chain direction and H-bond direction, respectively). The *shift "uncrossed"-chains* and *"crossed"-chains* stacking schemes as shown in Figure 3, parts b and c, are better than the *"uncrossed"-chains* stacking scheme as shown in Figure 3a. For EPP, EPA, EAP, and EAA, the unshifted *"uncrossed"-chain* structure in Figure 3a is 0.7−0.8 (kcal/mol)/(amide unit) higher than the other two.

In addition, the single H-bond sheet in EPP, EPA, EAP and EAA can slide in the chain direction by an integer number of *b*/7 with respect to the adjacent sheets, as shown in Figure 3.

Table 1. Free Energy ((kcal/mol)/(Amide Unit)) and Young's modulus (GPa) of Regular Crystal Structures of Nylon 6 at 300 K

SD*14/*b*		7	6	5	4	3	2	1	0	−1	−2	−3	−4	−5	−6
EAP α	*F*	50.61	50.99	50.62	50.77	50.63	50.76	50.66	51.22	50.79	50.75	50.71	50.78	50.66	50.01
	E_Y	295.8	257.5	285.5	294.6	294.6	284.6	267.3	293.1	268.2	283.4	294.6	294.4	285.2	263.4
EAA α	*F*	50.12	50.74	50.76	50.77	50.59	50.60	50.85	50.88	50.82	50.89	50.66	50.62	50.78	50.74
	E_Y	294.9	295.2	276.1	281.2	300.2	301.1	243.5	245.7	241.7	238.8	300.4	300.7	277.7	279.2
EPA δ	*F*	50.84	50.69	50.49	50.84	50.74	50.50	50.79	50.69	50.83	50.39	50.58	50.48	50.86	50.97
	E_Y	277.8	282.4	103.4	277.8	290.9	274.2	266.9	137.5	171.7	253.2	282.5	115.5	278.2	228.0
EPP	*F*	51.29	50.77	50.62	50.54	50.55	50.54	50.81	51.06	50.74	50.54	50.56	50.56	50.62	50.77
	E_Y	299.3	259.1	224.5	226.0	238.1	238.9	220.0	292.8	218.2	238.9	243.8	226.2	233.9	259.0
TAP γ	*F*								50.54						
	E_Y								135.0						
TPP	*F*								50.47						
	E_Y								153.6						

[a] There are eight amide units in the simulation unit cell as shown in Figure 2. [b] SD is the sheet displacement. For EPA and EAA, the definition of SD is a little tricky. We invert the adjacent sheet first and then define the sheet displacement *b* as the length of the unit cell in chain direction. [c] The free energy at 300 K is the sum of the zero point energy (ZPE), the potential energy and entropy at 300 K. [d] Young's modulus (GPa) is in the chain direction.

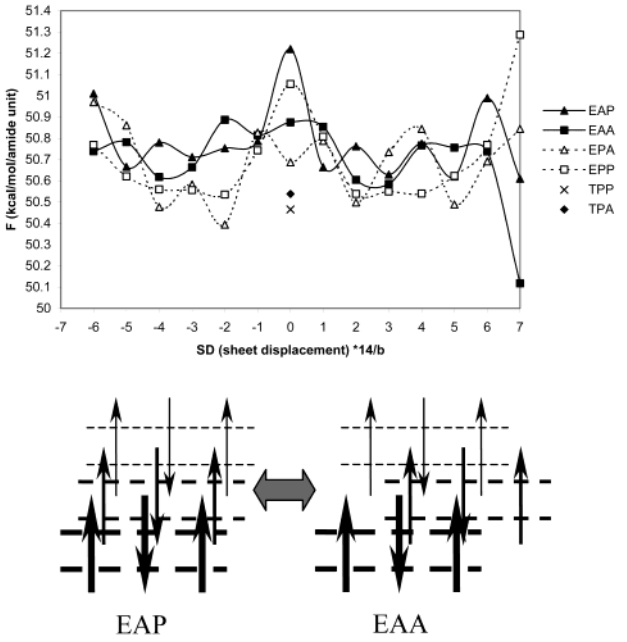

Figure 4. (a) Free energy of different infinite chain model structures at 300 K. (b) Transition between EAP and EAA.

Combining the 7 slides with *"crossed"* and *shifted "uncrossed"* leads to a total of 14 possible crystal model structures for each class (14 different sheet displacements).

Multiplying the 8 classes with the 14 stacking schemes (14 sheet displacements) leads to a total of 112 regular infinite chain crystal structures

3.3. Free Energy and Young's Modulus of All Possible Regular Crystal Structures of Nylon 6. We specified the space group of the simulated unit cell as[28] $P2_1$ and calculated the potential energy, ZPE (zero point energy), entropy, enthalpy, and free energy of all 112 regular crystal structures after energy minimization in PolyGraf 3.21. The unit cell and the atomic coordinates were optimized simultaneously. To compare the various model structures, we considered the free energy at 300 K. The results are listed in Table 1 and illustrated in Figure 4a. The parameters of the unit cell are listed in Table 2. When the SD (sheet displacement) in Table 1 is an odd integer, the crystal stacks with *"crossed"-chains* as in Figure 3c. When SD is even, the crystal stacks with *shift "uncrossed"-chains* as in Figure 3b.

Table 2. Unit Cell Parameters for Various Forms of Nylon 6 Crystal Simulated at 0 K and Experimental Structures at 298 K

crystal form	*a*/Å	*b*/Å	*c*/Å	*β*(angle)/deg
EAP-crossed	9.41	17.68	8.11	65.1
EAP-uncrossed	9.53	17.67	7.87	68.1
EAA-crossed	9.49	17.68	8.07	65.0
EAA-uncrossed	9.53	17.67	8.06	65.1
exptl α[6]	9.56	17.24	8.01	67.5
TPA	4.97	17.33	8.68	127.5
exptl γ[9]	4.78	16.88	9.33	121
EPA-crossed	4.72	17.67	7.91	114.6
EPA-uncrossed	4.77	17.67	8.75	122.0
exptl δ[23]		17.2		

3.3.1. EAP and EAA (α Form). First we consider the EAA and EAP classes, each of which has 14 models. All of these are denoted as α form. As shown in Figure 4b, EAP and EAA can transform to each other without difficulty. This transformation does not change the chain conformation and does not modify any hydrogen bonds. Thus, only vdW interactions are involved in the barrier, which is estimated to be 0.8 (kcal/mol)/(amide unit). Within the EAA and EAP classes, there are 14 possible model structures differing from each other by the sheet displacement, as shown in Figure 3. The 14 possible model structures can also transform to each other easily by overcoming the vdW energy barrier of about 0.7 (kcal/mol)/(amide unit).

For EAP the lowest free energy model is EAP+7 but there are two other models (+3, +5) with energies within 0.01 (kcal/mol)/(amide unit).

For EAA the lowest energy model is EAA+7 and it is 0.5 (kcal/mol)/(amide unit) lower than EAP+7. As shown in Figure 4a, EAA+7 is the best model structure and is roughly 0.4 (kcal/mol)/(amide unit) better than other models. In EAA+7, the coulomb interaction between the amide units of the adjacent H-bond sheets is significantly favored over that of the other models.

The model structure concluded by Holmes[6] from fiber X-ray (corrected by Simon[29]) to account for the α form is EAP±3, which is *not* consistent with the results here. However, after considering the fold structures in section 4.4, we find the same optimum crystal structure as Holmes.[6]

Leon et al.[30] reported results of rigid body sliding for infinite chains using the PCSP method to estimate interchain separations (PCSP does not minimize the energy of the conformation or cell for each displacement in our understanding). They calculate that the sheet

displacement with the most favorable potential energy is 4*b*/14. From relaxing the chains and unit cells we find that the most favorable is 7*b*/14. This indicates that it is important to relax the structures.

3.3.2. TPA (γ Form) and TPP. The pleating in the hydrogen-bonded sheets in TPP and TPA prevent them from sliding by b/7 with respect to the adjacent sheets. The only reasonable model structures are TPA+0 and TPP+0. For other sheet displacements, the TPP and TPA structures relax to EPP or EPA after energy minimization.

The TPA+0 model structure corresponds to the γ form, which is exactly the same as the model structure proposed by Arimoto.[9] The free energy is 0.4 (kcal/mol)/(amide unit) higher than EAA+7.

The free energy of TPP+0 at 300 K is very close to TPA+0 (the difference is only 0.07 (kcal/mol)/(amide unit)). But it is not possible to form a folded structure for TPP, since all chains are parallel to each other. Thus, TPP is not a reasonable regular crystal structure in the real fiber.

3.3.3. EPA (δ Form) and EPP. We denote EPA as the δ form. We find that EPA fits the X-ray characteristics of the metastable crystalline phase of nylon 6 described by Murthy.[23] He found that the fiber-axis diffraction scan of the metastable phase is similar to that of the α crystalline phase, but the equatorial diffraction scan is similar to that of the γ phase. We find the following points:

- EPA has the same *b* length (Table 2) as α form leading then to the same meridional scan,
- EPA has very similar *a*, *c*, and β angle parameters to the γ form (Table 2), leading thus to the same equatorial scan.

This agrees exactly with the experimental observations for the δ form. As discussed in section 3.4 below, EPA (δ form) accounts for an intermediate phase between α form and γ form (more precisely, between the β form and the γ form). The best model structure of EPA is EPA−2, which is 0.3 (kcal/mol)/(amide unit) worse than EAA+7.

The best model structure of EPP is EPP−2 and the free energy of EPP±2, EPP±3, and EPP±4 are almost indistinguishable. As with TPP, EPP has parallel chains so that it is not possible to form a folded crystal structure for the real fiber.

3.3.4. TAP and TAA. We find that TAP and TAA lead to high energies. Indeed the TAP and TAA unit cells relax to EAP and EAA with energy minimization. Keeping them rigid so that they cannot convert leads to energies 4 to 20 (kcal/mol)/(amide unit) higher than the other crystal forms. Such high energies make these structures extremely unlikely.

3.3.5. Young's Modulus. We predict a Young's modulus in the chain direction of 295 GPa for α, 135 GPa for γ, and 253 GPa for δ. The value for α is above the experimental value[31] of 168 GPa, because the experimental system has finite thickness lamellae, disorder in the chain conformation, and imperfections.

3.4. *Intramolecular* and *Intermolecular* Hydrogen bonds and the Thermostability of the α Form over Other Forms. Since the molecular weight of a nylon polymer is large, we consider that each lamella involves the same polymer chain folded repeatedly (of course there may be more than one polymer chain in a lamella, and the polymer chain in one lamella may exit the lamella and connect through an amorphous region to an adjacent lamella or back to the same one). Each such covalently connected polymer chain we will consider as one *molecule*. For an isolated molecule, we would expect the chain to fold repeatedly to allow intramolecular hydrogen bonds, denoted hereafter as: *intra-H-bonds*. Folding an isolated polymer chain to form *intra-H-bonds* necessarily leads the adjacent chain to be in opposite directions. Thus, *intra-H-bonds* are always between antiparallel chains.

It is also possible to have crystals in which the hydrogen bonds are between different molecules or between remote parts of the same molecule. We will denote this case of intermolecular hydrogen bonds as *inter-H-bonds*.

The lowest enthalpy for a folded molecule with *intra*-H-bonds would lead to a 2D sheet with a constant length between folds. Two such sheets could be packed to form a 3D structure where the intermolecular interactions would be dominated by van der Waals (non-Coulomb) interactions since that H-bonds are all within sheets. As discussed in section 4 (below), this packing leads to the α structure of nylon, which is the most stable crystal structure for nylon 6.

An alternative packing is to start with the above structure having parallel sheets of intramolecular bonds and rotate the amide groups to make hydrogen bonds to the molecule in the adjacent sheet, leading to *inter-H-bonds*. As discussed in section 4 (below), this packing leads to the γ structure of nylon-6, which can be formed experimentally from the α structure by iodination. Also we will find that the δ form has only *inter-H-bonds*.

Thus, for nylon 6, when H-bonds are parallel with the fold direction, the H-bonds are intramolecular. Otherwise, the H-bonds are intermolecular. Prior to crystallization we would expect *intra H-bonds* to be favored since this does not require that the motions of different molecules be correlated. Thus, we would expect nucleation and growth from solution to be dominated by molecules containing *intra-H-bonds*. The energetics of individual molecule for nylon 6 are discussed in section 4.3. The recent simulations by Welch and Muthukumar[32] support this role of *intra-H-bonds*. They conclude that: "Lamella thickening is a highly cooperative process requiring the mobility of all chains in the crystals."[32] Obviously, *intra-H-bonds* favor molecular mobility, and formation of the H-bond sheet inside the molecule is enthalpically favored. These considerations lead to the conclusion that *intra-H-bonds* are favored over *inter-H-bonds*, both energetically and kinetically from solution. However, assuming 90% H-bonds are formed in amorphous region from melt and most of them are *inter*-H-bonds, γ form is kinetically favored. These *intra-H-bonds* account for the thermostability of the α form over all other forms.

3.5. Transition Mechanism and Intermediate β Form, δ Form between α Form, and γ Form. 3.5.1. Fiber X-ray Results for Intermediate Forms in the Literature. After the elucidation of the structures for the α form and γ form of nylon 6,[6,9,33] many studies have examined the crystalline phase intermediate between α and γ.[12,13,16−24] The intermediate phase is normally observed in fibers under stress, but has been observed in relaxed fibers, and it can be transformed into either the conventional α form or γ form using suitable thermomechanical treatments. For example, stretching the fibers up to their breaking points[12,13] or boiling in

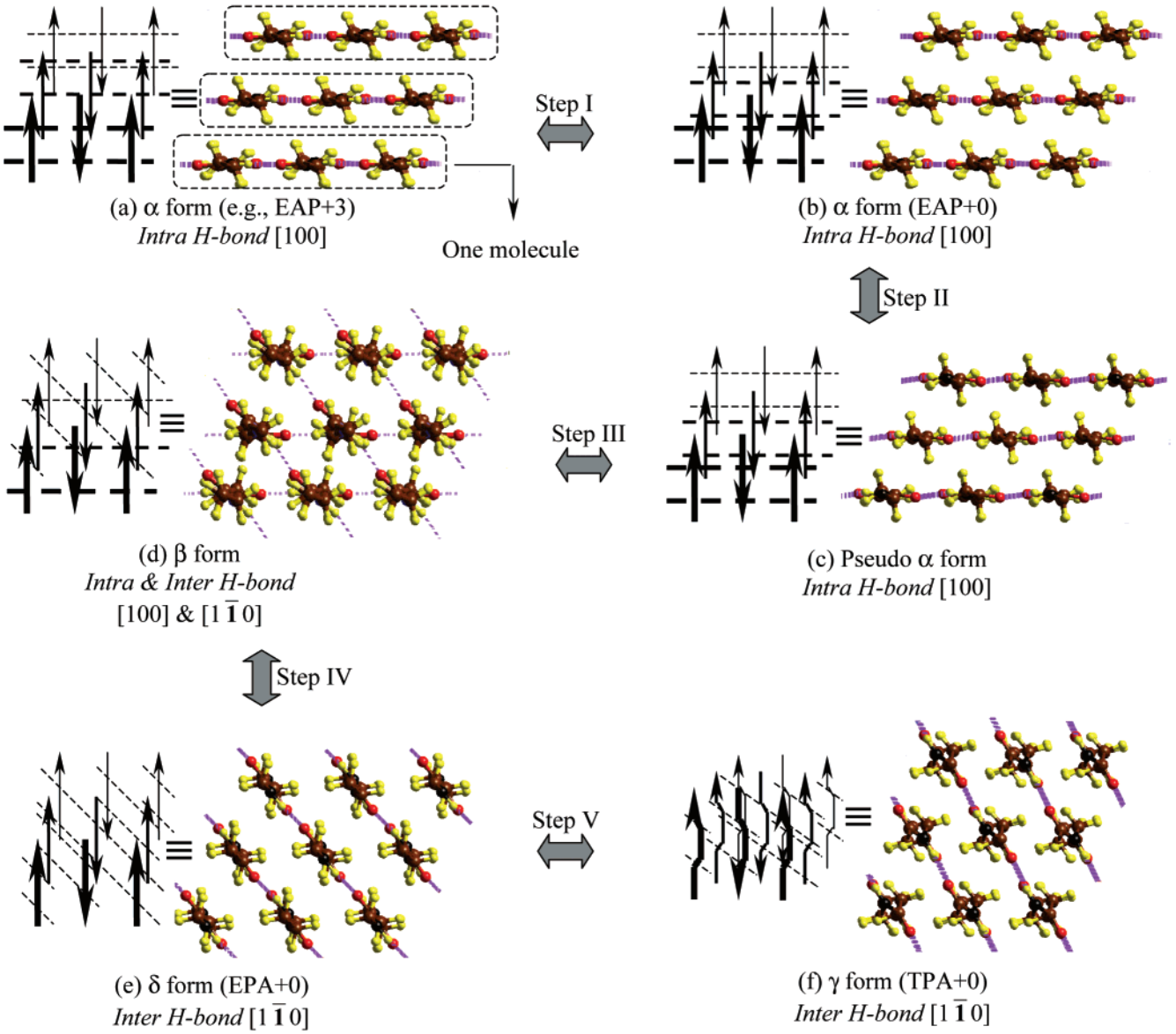

Figure 5. Transition mechanism and metastable forms between α and γ forms.

water at temperatures between 100 and 160 °C[12,13,34] transforms the intermediate phase to the α form.

Holmes[6] discussed an unstable structure that he denoted as the β form. The very obvious difference between β form and α form is that the meridional spot 020 of fiber X-ray (barely visible in the α form) is the strongest spot in the fiber diffraction for the β structure.

Murthy[23] pointed out that the fiber-axis diffraction scan of the metastable phase is similar to that of the α crystalline phase, while the equatorial diffraction scan is similar to that of the γ phase.

Recent fiber X-ray results of Auriemma et al. [24] show that the mesomorphic form is made of small mesomorphic aggregates of chains and the chains have disordered conformations with the H-bonds are formed in different directions. They consider the term mesomorphic to refer to the phase intermediate between α form and γ form. As discussed below we consider there to be three distinct intermediate phases. The one discussed by Auriemma is the one often referred to as β.

3.5.2. Steps in the Transformation between the α Form and the γ Form. The transformation between the α form and the γ form cannot be a direct single step process because it requires breaking a number of H-bonds, making a number of new H-bonds, and changing chain conformation.

On the basis of the results in section 3.3 and the fiber X-ray results in section 3.5.1, we propose five detailed transformation steps between the α form and the γ form as illustrated in Figure 5. Figure 5 represents the different forms by showing nine chains of nylon 6, consisting of three molecules. The folds connecting chains with each other are circled in Figure 5a to help understand the composition of the chains in terms of molecules.

♦ Step I from Figure 5a to Figure 5b: The H-bond sheet in the α form slides (by 3*b*/14) in the chain direction with respect to adjacent H-bond sheet. In Figure 5a, the amide units in the adjacent H-bond sheets (adjacent molecules) are not on the same height. By overcoming the 0.7 kcal/mol (amide unit) vdW energy barrier (see section 3.3.1), the adjacent H-bond sheet can slide to keep the amide units on the same height as shown in Figure 5b.

♦ Step II from Figure 5b to Figure 5c: All of the amide units are twisted ~10° with respect to the two connected

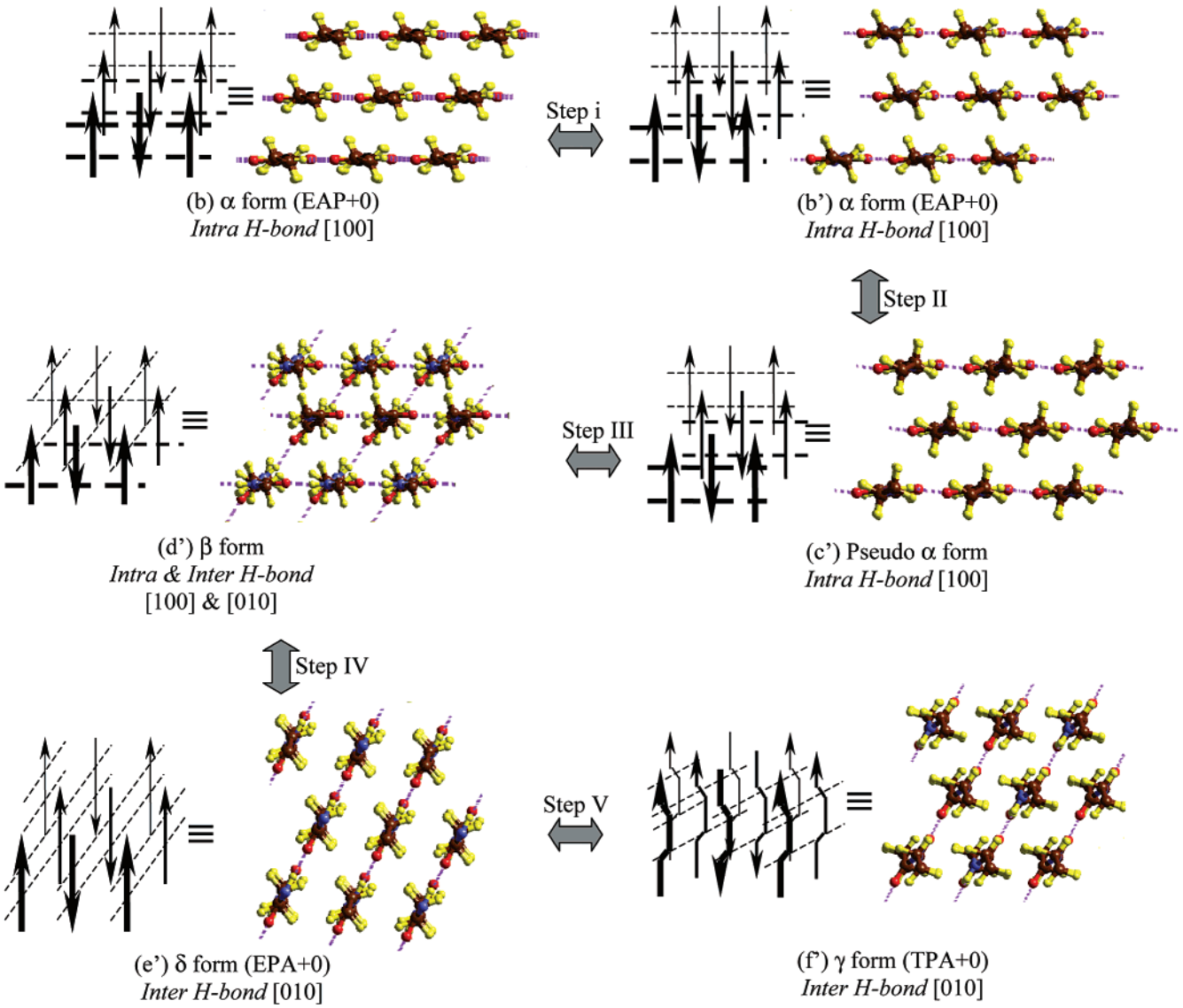

Figure 6. Alternative version of the transition mechanism in Figure 5.

pentamethylene segments while preserving the H-bonds. This structure is similar to α, but has a slightly different chain conformation.

♦ Step III from Figure 5c to Figure 5d: Starting from Figure 5c, we break half of the *intra-H-bonds* in the [100] direction and form new *inter-H-bonds* in the [1$\bar{1}$0] direction while retaining the other half of the *intra-H-bonds* in the [100] direction. This structure is similar to the *β* form proposed by Auriemma[24] and to the interphase form proposed by Murthy.[23]

♦Step IV from Figure 5d to Figure 5e: The remaining *intra-H-bonds* are broken while forming *inter-H-bonds*.

♦ Step V from Figure 5e to Figure 5f: The pentamethylene segments rotate as rigid bodies with respect to the amide units so that the chain conformation changes from extended to twisted.

An alternative pathway, which is shown in Figure 6, from α to *γ* is in step i to slide the middle H-bond sheet with respect to the upper and lower ones by *a*/4 in the hydrogen bond direction to form Figure 6b′ (Figure 6b shows the same structure as Figure 5b). Then in step III the half of the amides that twist do so in the opposite direction ([010] for original α form) to form Figure 6d′. In this case the step IV leads to a *δ* form with the hydrogen bonds in this same [010] direction. Then step V leads to *γ*, but with the hydrogen bonds in the [010] direction.

3.5.3. *β* Form. We find that the structure in Figure 5d fits the fiber X-ray results from Holmes,[6] Ziabicki,[15,16] and Auriemma.[24] Following their notation,[6,15,16,24] we name the structure in Figure 5d (Figure 6d′) as the *β* form. Because the amide units are on the same height in the structure of Figure 5d (Figure 6d′), they give a periodicity of 0.835 nm (the 010 spot), which is consistent with the fiber X-ray result from Auriemma.[24] We consider this same structure to be responsible for the strong 020 diffraction observed by Holmes,[6] who reported a periodicity of 0.862 nm.

The structures of Figures 5d and 6d′ have H-bonds formed in three distinct directions leading to disorder in the chain conformation. These hydrogen bonds would be in the [100], [1$\bar{1}$0], and [010] directions as discussed above, which is consistent with the conclusion of Auriemma[24] from fiber X-ray results.

3.5.4. *δ* Form. The structure in Figure 5e (Figure 6e′) corresponds to the regular crystal structure EPA+0 discussed in section 3.3.3. We denote this as the *δ* form

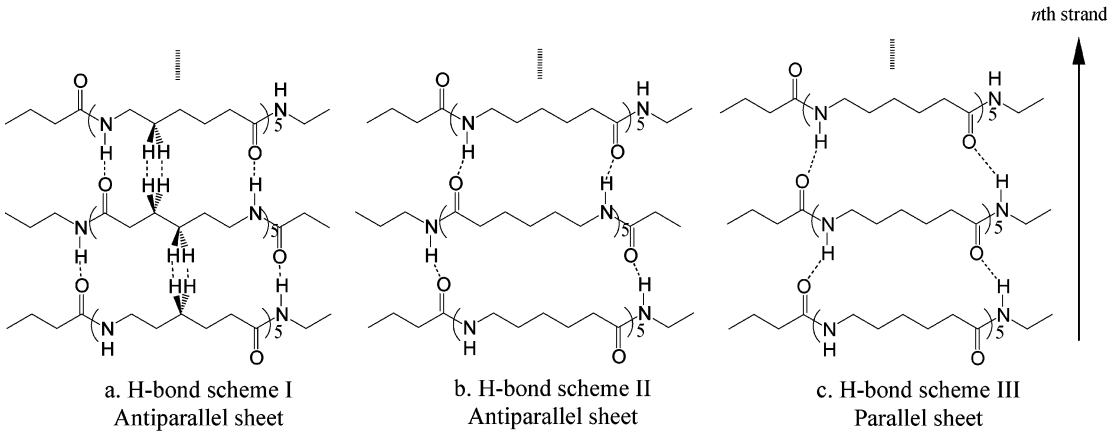

Figure 7. Three H-bond schemes for H-bond sheets. (Illustrated is the three strand case with six formula units in each strand.)

Table 3. Energy for the H-Bond Schemes Shown in Figure 7 Using the MSXX FF[a]

	E (kcal/mol/amide unit)		
	H-bond I	H-bond II	H-bond III
Val	30.644	30.592	30.656
VdW	4.321	3.388	3.217
electrostatic	−70.005	−69.605	−69.534
total	−35.040	−35.625	−35.661

[a] The *c* length of the unit cell is restricted to 50 Å.

because it fits the fiber X-ray results of the intermediate phase observed by Murthy.[23] (see section 3.3.3)

From Figure 5 (Figure 6) and section 3.3.2, we can now understand the characteristics of intermediate phase from Murthy.[23] The difference between δ form and α form results from a different H-bonds pattern. The difference between the δ form and the γ form results from a different chain conformation. Both the α form and the δ form are composed of extended chains, leading to a Young's modulus much larger than the γ form, which is composed of pleated chains. Thus, Table 1 shows that Young's modulus for the γ form's (TPA) is lower than EPA (the δ form) and lower than EAA, EAP (α form). It is reasonable that stretching the γ form would lead to the full-extended chains of the δ form (EPA), as found by Murthy.[23]

3.6. The H-Bond Schemes in the α Form (EAP, EAA), the δ Form (EPA), and EPP. It is well accepted[6] that for nylon 6, all H-bonds are made perfectly between antiparallel fully extended chains as shown in Figure 7a. For parallel full-extended chains (Figure 7c), the H-bonds cannot be made perfectly due to the bad H-bond angle.[6] Thus, the H-bond scheme III in Figure 7c is worse than the H bond scheme I in Figure 7a. However, we find that the H-bond scheme I is worse than schemes II and III by 0.6 (kcal/mol)/(amide unit) (see Table 3).

There are two reasons for this.

There is a bad contact between the pentamethylene units. Bad contact exists between 10 hydrogen atoms of every repeating unit as shown in Figure 7a. From Table 3, we see that the vdW part of H-bond scheme I in Figure 7a is 1.0 (kcal/mol)/(amide unit) worse than in schemes II and III, as shown in Figure 7b and 7c.

Although a linear H bond is best, the energy cost of small displacements from linear is small. Thus, Table 3 shows that the electrostatic part for H-bond scheme I is 0.4 (kcal/mol)/(amide unit) better than those for Figure 7, parts b and c, because of better H-bonds.

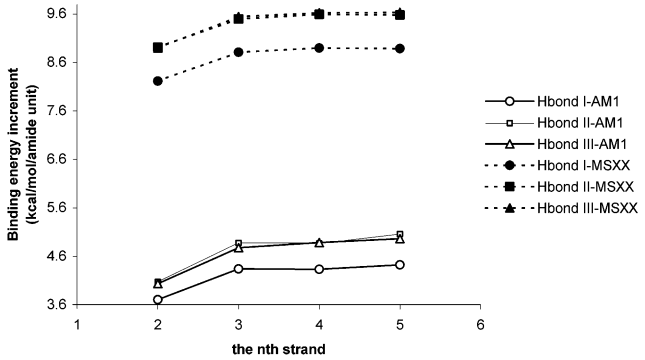

Figure 8. Binding energy increment per amide, $\epsilon_n = E_n = [E_{B(n)} - E_{B(n-1)}]/6$, for adding the *n*th strand calculated using AM1 and MSXX FF.

3.6.1. Validation of the FF Results. To corroborate these results from the FF, we used semiempirical QM calculations (AM1) to compare the binding energy of different H-bond schemes in Figure 7.

Using AM1, we first optimized a single chain containing six amides (as shown in Figure 7) with the backbone atoms fixed on the same plane. Then we performed rigid body minimization of the dimer, trimer, etc. until the fifth strand. This was done for the three H-bond schemes shown in Figure 7 for a three-strand case. Defining $E_{B(n)}$ as the total binding energy with *n* strands, then we consider the following points:

• $E_n = E_{B(n)} - E_{B(n-1)}$ is the incremental binding energy (per amide) for adding the *n*th strand

• $\epsilon_n = E_n/6$ is the average binding energy increment for each amide of the *n*th strand.

Figure 8 shows the ϵ_n results for each of the three different H-bond schemes. Here we see that ϵ_n is about the same for $n \geq 3$, but is about 1 kcal/mol weaker for $n = 2$. This suggests a cooperative component to the hydrogen bonding. We see that H bond Figures 2 and 3 (with bent hydrogen bonds) are competitive while H-bond scheme I (with linear hydrogen bonds) is 0.5 (kcal/mol)/residue worse than II and III. This result confirms our MSXX FF result in Table 3.

Similarly, we use MSXX FF to get the binding energy increment as shown in Figure 8. MSXX FF gives us similar conclusions except that the absolute binding energy is higher than that from AM1 due to the different charges. By analyzing the energy components of our MSXX FF calculations, we conclude that the cooperative component arises from coulomb interaction.

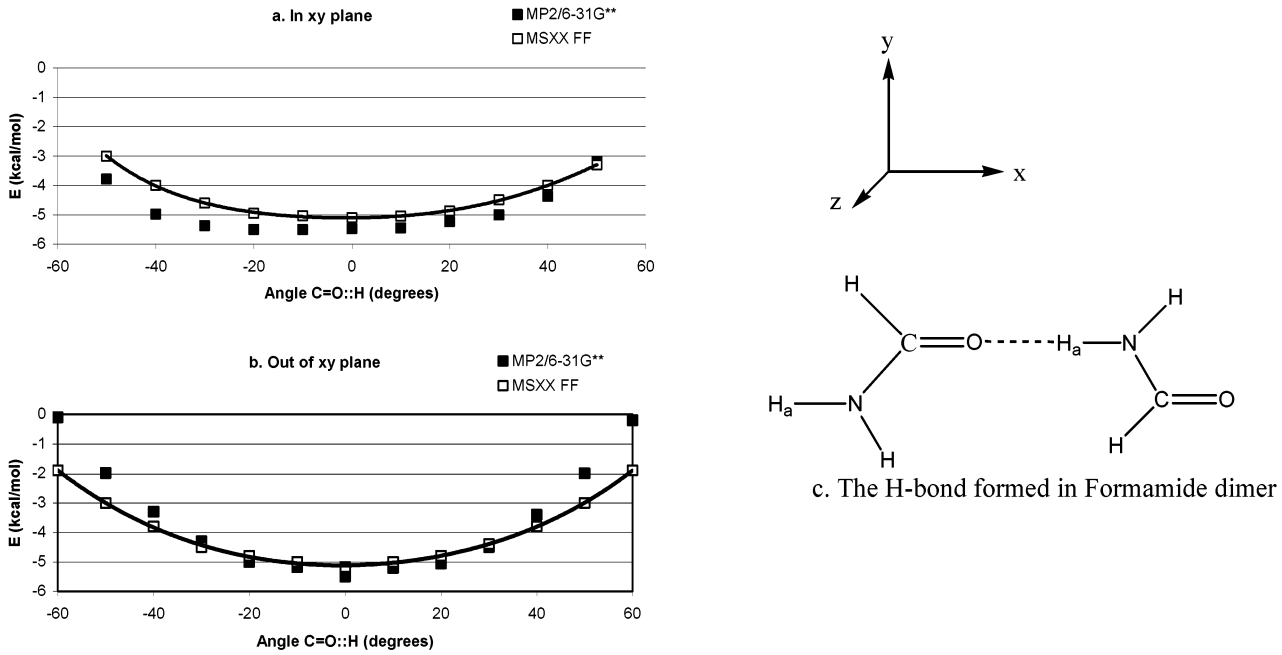

Figure 9. Dependence of the bond energy Formamide dimer on H-bond angle for translation of one amide unit relative to the other (a) in the *y* direction (in plane) and (b) in the *z* direction (out-of-plane) (based on Figure 4 of ref. 3).

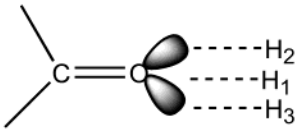

Figure 10. Schematic of the hydrogen bond with different COH angles.

3.6.2. Dependence of H-Bond Energy on H-Bond Angle. To understand how the H-bond energy depends on the linearity of the bond, we show in Figure 9 the change in the binding energy of formamide dimer as one formamide is translated in the plane of the dimers (Figure 9a) or perpendicular to the plane (Figure 9b). Here we compare the results for the MSXX FF with ab initio QM at the MP2 level. This shows that MSXX FF gives a good description of QM.

Figure 9a shows that the potential for in-plane sliding (the *y* direction) is quite soft. One can understand this in terms of the sp^2 lone pairs of the carbonyl (see Figure 10) which lead to significant electronic density extended from the oxygen in the *y* direction, making the interaction energy with the partially positive H favorable for displacements (2 kcal/mol for 50°).

In contrast the electron density at the oxygen drops off quickly in the *z* direction so that displacement in the out-of-plane *z* direction results in a much stiffer potential (3 kcal/mol for 50°; see Figure 9b).

The soft in-plane sliding and the packing effects between methylene units make the H-bond in Figures 2 and 3 ~0.5 kcal/mol better than I in Figure 7. QM calculations (HF-6-31G*) on optimized glycine β-sheet structures also lead to nonlinear H-bonds as in II and III over the linear ones as in I.[35]

3.7. The H-Bond in γ Form. It is well accepted that, for nylon 6, the γ form is not as stable as the α form.[9,23,33] On the other hand, Hatfield et al.[1] concluded, from the results of solid-state ^{13}C and ^{15}N NMR experiments, that the H-bond in the γ phase is stronger than that in the α phase. We believe that rather than measuring bond strength, their result is related to the shielding of the amide proton, which is probably related to the linearity of the hydrogen bond.

Our simulation results show that the angle C═O::H in the γ phase is more linear than that in the α phase. Thus, we found this angle to be 170.7° in the γ form (TPA+0) and 156−158° in EAP (α form) and EAA (H-bond scheme II in Figure 7b), and 153° in EPA (δ form) and EPP (H-bond scheme III in Figure 7c).

A linear H-bond angle should lead to the biggest effect on the charge distribution in the amide units, which should directly affect the chemical shifts observed by solid-state NMR.

3.8. Comparison with Fiber X-ray Results. We used the "Diffraction-Crystal" module in Cerius^2 4.0 to calculate the fiber X-ray diffraction and to obtain the *R*-factor with respect to the experimental data.[6,9]

We calculated the *R*-factor of 28 model structures of EAP and EAA with respect to the intensity data of the α form from Holmes.[6] The calculated *R*-factors range from 0.258 to 0.408. In this calculation the mean squared atomic displacements used for the temperature factor are $\langle a^2 \rangle = 0.39$ Å^2, $\langle b^2 \rangle = 0.08$ Å^2, and $\langle c^2 \rangle = 0.46$ Å^2, which we derived from *NVT* molecular dynamics.

The analysis of the critical intensities such as 020 gives a conclusion similar to those derived by Holmes.[6] The intensity of 020 becomes close to zero when the sheet displacement is $^3/_{14}b$ or $^4/_{14}b$ (2.9 and 3.9 Å, respectively). Otherwise, the intensities/ratios of 020 range from 24/2.4% to 61/6.1%, which differs from the observed intensity, 1/0.1%.[6] The calculated intensities/ratios of different sheet displacements for 020 and 040 are listed in Table 4. Holmes suggested that the 3*b*/14 sheet displacement is best because the similarly charged polar groups will be uniformly distributed along the *b*-axis rather than close to each other as they are in nylon 66. Instead we find that the best crystal structure for infinite chains (see Table 1) is EAA+7 and not EAP+3. In section 4.4, we discuss the effects of having finite thickness lamella, where we find the interactions between the folds lead directly to the 3*b*/14 sheet displacement.

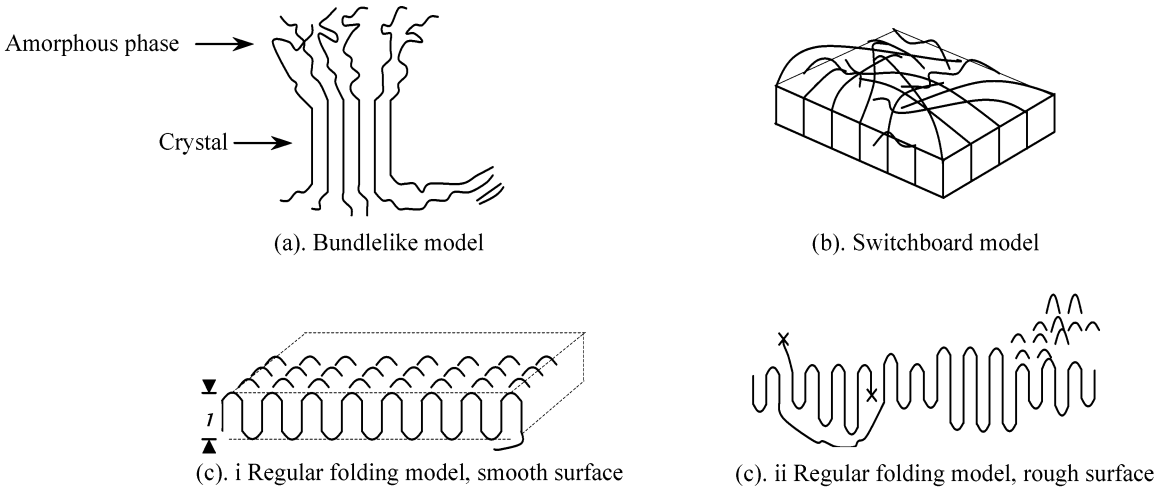

Figure 11. Schematics for suggested fold models of polymer crystals (based on Figure 2 of ref. 34).

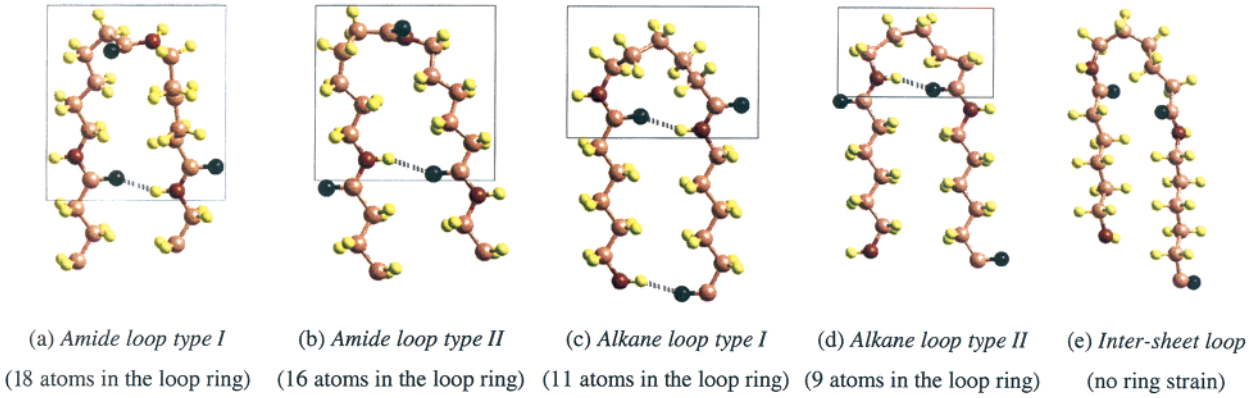

Figure 12. Five types of loop structures for nylon 6.

Table 4. Calculated (020) and (040) Intensities/Relative Ratios for Different Sheet Displacements of EAP, Compared to Experiment[6]

SD *14/*b*	0	−1	−2	−3	−4	−5	−6	exper
020	60.3/6.1%	49.5/5.1%	25.3/2.6%	3.1/0.3%	2.2/0.2%	23.3/2.4%	47.5/5.0%	1/0.1%
040	20.6/2.1%	8.7/0.9%	0.5/0.1%	17.2/1.8%	17.9/1.9%	1.2/0.1%	6.6/0.6%	6/0.6%
SD *14/*b*	1	2	3	4	5	6	7	
020	49.0/5.0%	21.6/2.2%	2.9/0.3%	3.9/0.4%	23.9/2.4%	50.5/5.1%	60.7/6.1%	
040	8.0/0.8%	1.8/0.2%	17.8/1.8%	15.6/1.6%	0.9/0.1%	9.5/1.0%	21.6/2.2%	

We find that for infinite chains all EAP and EAA structures lead to a significant discrepancy in the intensities of the seventh layer line, as originally mentioned by Holmes.[6] Displacing the sheet by *b*/7 as shown in Figure 3 does not affect the intensities of the seventh layer line. However, the "uncrossed" and "crossed" structures shown in Figure 3, parts b and c, give quite different intensities of the seventh layer line. The "uncrossed" structure gives significant intensities for *h*7*l* with even *l* while the "crossed" structure gives significant intensities for odd *l*. Unfortunately, Holmes[6] listed odd *l* of *h*7*l* only for observed intensities. For this reason the "uncrossed" structure leads to a larger *R*-factor than the "crossed" structure. We explain the discrepancies for the seventh layer line to the coexistence of "crossed" and "uncrossed" structures.

4. Results and Discussion for Folded Structures (Lamella) of Nylon 6

4.1. Introduction. It is generally accepted that many linear polymers form crystalline regions or lamella consisting of folded chains. This includes polyethylene, polyoxymethylene, poly(ethylene terephthalate), and nylon. Three models of chain-folded polymer crystals have been proposed[36] as shown in Figure 11: (a) the fringed micelle or bundlelike model; (b) the random reentry or "switchboard" folded model; (c) the adjacent reentry chain-folded models (regular folding, smooth surface).

Models a and b would lead to substantially low total densities. Model c of lamellae with smooth surfaces would lead to a total density close to the X-ray crystal density. Model d of lamellae with rough surfaces would be expected to have some voids or bubbles between the lamellae, leading to a density somewhat below the X-ray crystal density.

The measured density of the piece of the monofilament nylon 6 used for the intensity measurements was[6] 1.160 ± 0.001 g/cm^3, which is quite close to the crystal density of 1.233 derived from the X-ray unit cell[6] (a = 9.56 Å, b = 17.24 Å, c = 8.01 Å, β = 67.5°). For the regular lamellae model we constructed, we find a density at 0 K of 1.18 ± 0.02 g/cm^3 (the uncertainty depending upon which types of loops are used). The good agreement with experiment strongly suggests that the

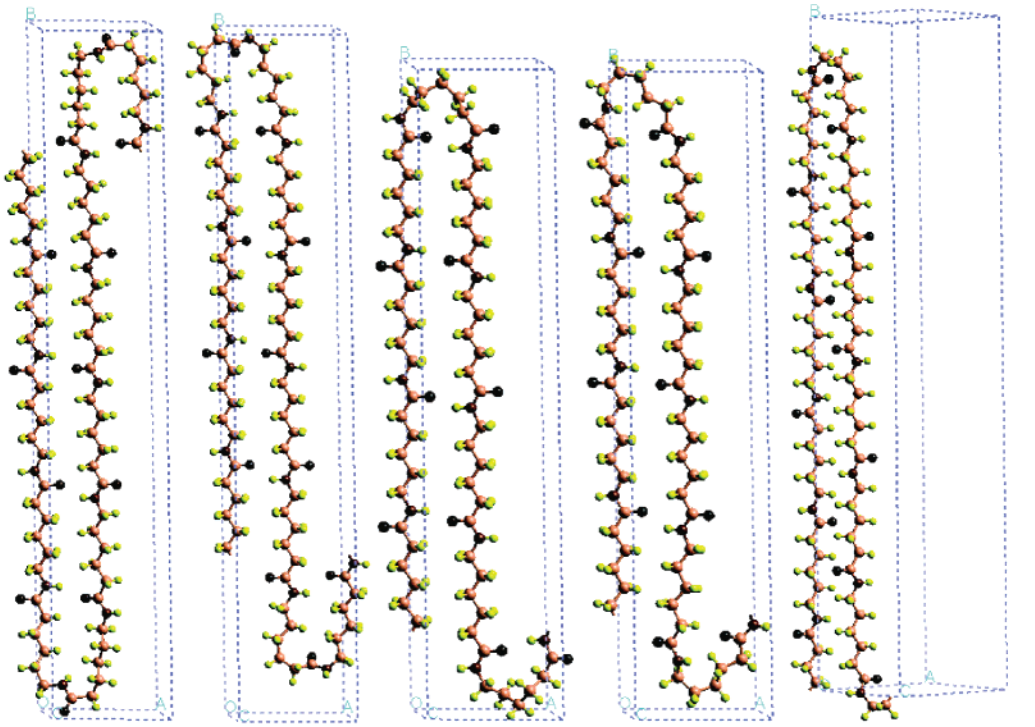

Figure 13. Individual molecules of five different types of loop structures.

experimental system has a regular lamella structure as in Figure 11c.

4.2. Different Types of Loops for Nylon 6. There are five types of loops for the lamella with smooth surface shown in Figure 11c. The loop can be formed (a) with *intra-H-bonds* leading to the four cases in Figure 12a−d or (b) with *inter-H-bonds* (*intersheet*, Figure 12e).

For the first four loops must be compatible with forming the H-bonds (dotted lines in Figure 12a−d), leading to a ring constraint. This can be done in two ways:

•Two amide units to form the loop (Figure 12, parts a and b), denoted as the *amide loop*.

•One amide unit to form the loop (Figure 12, parts c and d), denoted as the *alkane loop*.

The loop ring of the *amide loop* includes 18 atoms (Figure 12a, type I) or 16 atoms (Figure 12b, type II), whereas the *alkane loop* has 11 (Figure 12c, type I) or 9 (Figure 12d, type II).

Thus, the *amide loop* leads to less ring strain than the *alkane loop*, but the *alkane loop* has one additional amide unit in the stem chain for favorable hydrogen bonding and packing. For both *amide loop* and *alkane loop*, there are two cases referred to as type II. Type II has two less atoms in the loop than type I leading to a stiffer more highly strained loop.

In contrast, the *intersheet loop* (between H-bond sheets) leads to very little constraint on the loop ring. In addition, it uses only one amide unit in the loop, just as for the *intrasheet alkane loop*. For comparing the *intersheet loop* case with the various *intra-H-bond* cases, we selected the lowest energy intersheet H-bond case.

To determine the energetics for different types of loops, we performed NVE molecular dynamics (MD) of the model structures shown in Figure 12. MD is necessary to allow the loops to achieve their most favorable shape. In these calculations, we fixed the stem regions, allowing only the atoms in the loop to move. To be consistent we included the interactions among the 57 atoms shown in Figure 12 but allowed only the ones in the boxes to move in the dynamics. We then performed a total of 1 ns MD using a 1 fs time step at 600 K. Then we analyzed the 20 potential energy lowest frames and minimized them to get candidate structures for the optimum structure of each type of loop. MD of the whole system will give a better analysis in cost of a lot of computer time. By using the strategy described above, in which MD is performed before energy minimization, we get reasonable results in cost of normal computer time.

Next we must consider how thick to make the lamellae. Considering oligomers of nylon 6 containing just 10-amide units,[37] the lamella stacking periodicity (LSP) from X-ray diffraction is 4.77 ± 0.05 nm. Such systems will fold just once, suggesting a lamella thickness for nylon 6 that is 2.8 times the *b* length of the original unit cell[6] (17.24 Å). Trifan et al.[38] showed from X-ray experiments that the lamella thickness of nylon 66 is approximately 58 Å (that is 3.3 times the b spacing) and independent of the bath temperature. The optimum lamella thickness involves a balance of thermodynamics and kinetics. Thick lamella leads to increased stability but the kinetics limits the growth rate thick lamella (requiring the long chains to be aligned as the crystal grows). On the basis of these experimental results, we decided to aim at a lamella thickness of ∼50 Å.

To use just one type of loop for *intrasheet loop* cases, it is necessary to have an even number of amides in each stem. To achieve a thickness of ∼ 50 Å leads to the choice of four amides per stem for *alkane type* and five amides per stem for *amide type*.

4.3. Optimum Loop Type for Individual Molecules. First, we consider the optimum loop type for the individual molecules shown in Figure 13. To eliminate intermolecule interactions we fixed the distance

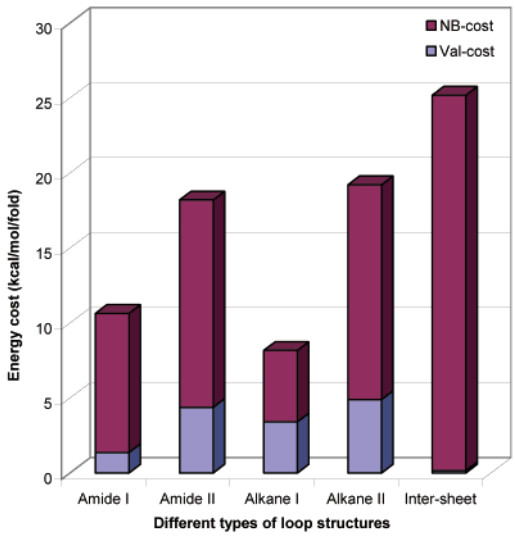

Figure 14. Energy cost of different types of loops in individual molecule.

Table 5. Unit Cell Parameters of Nylon 6 Lamella Crystal after Minimization at 0 K

fold type of lamella	*a*/Å	*b*/Å	*c*/Å	β(angle), deg
amide I	9.42	53.58	8.45	64.5^o
amide II	9.43	54.10	8.03	72.9^o
alkane I	9.38	44.03	8.11	70.0^o
alkane II	9.37	44.20	8.06	73.4^o
intersheet	9.47	53.74	8.24	64.8^o

Table 6. Energy Cost Different Types of Fold in Individual Molecule and 3D Lamella Crystal (SD = $^3/_{14}b$) ((kcal/mol)/Fold)

fold type	amide I	amide II	alkane I	alkane II	intersheet
individual molecule	10.625	18.194	8.164	19.202	25.173
3D lamella	16.432	25.335	12.107	28.790	6.809

between layers (molecules) to be 50 Å, and we fix the LSP (b length of the unit cell) to be 100 Å.

The energy cost of forming the various types of loops for individual molecules is shown in Figure 14 and Table 6. The fold energy cost is normalized by the number of folds. The reference energy is a single H-bonded sheet formed between infinite antiparallel chains without a fold (the distance between sheets again fixed at 50 Å). This MSXX FF energy is −35.940 (kcal/mol)/(amide unit).

The energy cost of the fold part arises from two terms:

- *Nonbond part* (packing energy cost).
- *Valence part* (ring constraint cost).

The cost of losing the H-bond is included in the *nonbond part*. Here we see that the *alkane loop type I* is best, with a cost of 8.2 (kcal/mol)/fold, next is *amide loop type I* (10.6), then *amide loop type II* (18.2), and then *alkane loop type II* (19.2).

The difference between *amide loop type I* and *alkane loop type I* is 2.4 (kcal/mol)/fold, which is less than one H-bond. For both *amide loop* and *alkane loop*, *type II* is always worse than *type I* because of the additional ring constraint in *type II*.

For the *intersheet loop* case, the individual molecule energy is much less favorable (by ∼17 (kcal/mol)/fold; see Figure 14) than the *alkane loop type I* case, because of the lack of H-bonds. We see from Figure 14 that the energy cost for one molecule of *intersheet loop* almost comes from the *nonbond part* (mainly H-bond part).

(a) *Loop stacking type I* (b) *Loop stacking type II*

Figure 15. Two ways of stacking adjacent loops. (The fold structure is projected down the chain axis. The wave line and the small circle represent the loop and the straight stem segment, respectively.)

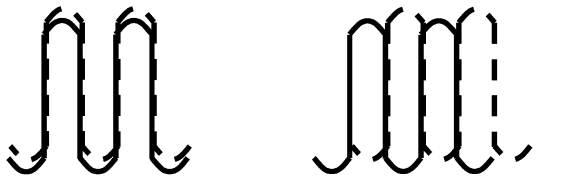

(a) *Eclipse fold-sheet stacking* (b) *Staggered fold-sheet stacking*

Figure 16. Two ways of stacking adjacent fold sheets.

(a) *Eclipse lamella stacking* (b) *Staggered lamella stacking*

Figure 17. Two ways of stacking the adjacent lamellae.

Thus, the *intersheet loop* is not favored for individual molecules and is not favored by dynamics.

Jones et al.[37] discussed the "*amide fold*" and two types of "*alkane fold*" for singly folded finite chains of nylon 6 using the CVFF force field. They concluded that the "*amide fold*" and one of the two "*alkane folds*" are both good folds for nylon 6. However, they did not provide any details of the fold energy cost.

4.4. The Stacking of the Fold Sheets and the Best Fold Sheet Displacement. 4.4.1. Two Best of Eight Possible Stacking Schemes for Folded Sheets. Before going to 3D lamella crystal structures, we will first consider all possible stacking schemes of the folded sheets.

Because the loop parts of folded sheets are wavelike, there are two ways of stacking the adjacent loops, as shown in Figure 15. We call them *loop stacking type* I and *loop stacking type II*, respectively. *Loop stacking type I* is better than *loop stacking type II*, because there is less vdW repulsion energy between the adjacent loops. The energy difference between them varies depending on the fold sheet displacements and the way of stacking the folded sheets. In the following calculations we will consider only *loop stacking type I*.

Besides the two ways of stacking of adjacent loops shown in Figure 15, there are two ways of stacking folded sheets in the H-bond direction as shown in Figure 16. We call these *eclipse fold-sheet stacking* and *staggered fold-sheet stacking*, respectively.

In addition, considering the stacking of the folded sheets in the chain direction, there are two ways of stacking the lamella, as shown in Figure 17. We call these *eclipse lamella stacking* and *staggered lamella stacking*. The difference between them and the conver-

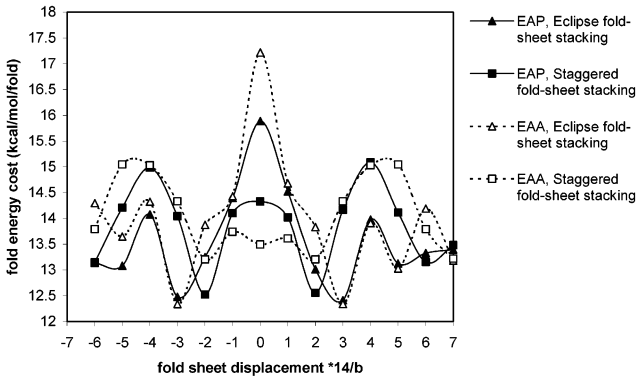

Figure 18. Fold energy cost for different sheet displacements of *alkane loop type I*.

sion between them involves only loop vdW interactions. For the folded sheets of *alkane loop type I* shown in Figure 12c, *eclipse lamella stacking* is better than *staggered lamella stacking* by 0.422 (kcal/mol)/fold (keeping the c length still fixed at 50 Å).

Different lamella stacking type gives different optimum *b* spacing. For the folded sheets of *alkane loop type I*, *staggered lamella stacking* gives 45.3 Å, which is 1.3 Å larger than for *eclipse lamella stacking*.

To be consistent, all the unit cells simulated below are constructed using *eclipse lamella stacking*.

From Figures 15−17, there are total $2^3 = 8$ possible stacking schemes for folded sheets. We will consider just the two best of them.

4.4.2. Folded Sheet Displacements. The folded sheets can slide in chain direction with respect to adjacent sheets just like the infinite chain model structures discussed in sections 3.2 and 3.3. Figure 18 gives the fold energy cost dependence on the fold sheet displacement. The reference energy here is the energy of EAP+3 infinite chain model structure in Table 1. Thus, the "fold energy cost" in Figure 18 includes both the energy cost of converting stem amide units into loop units and the energy of stem segments sheet displacement in chain direction.

For both EAP and EAA we find that the best displacement for *eclipse fold-sheet stacking* is $^3/_{14}b$. Two factors affect the fold sheets stacking.

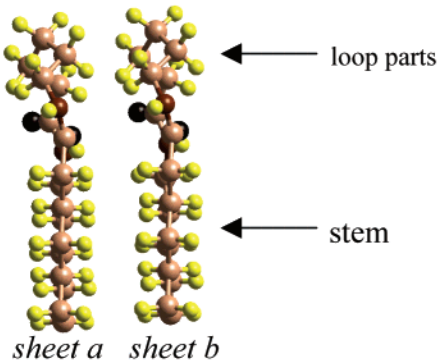

a. The fold sheet displacement is zero. There is strong vdw repulsion between the folded parts, but the packing of the stem parts is good.

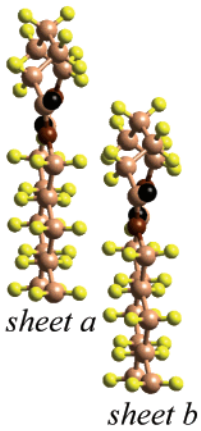

b. The fold sheet displacement is $3b/_{14}$. The amide part in *sheet a* provides much space for the folded part in *sheet b*.

Figure 19. Various fold sheet displacements of *eclipse fold-sheet stacking*.

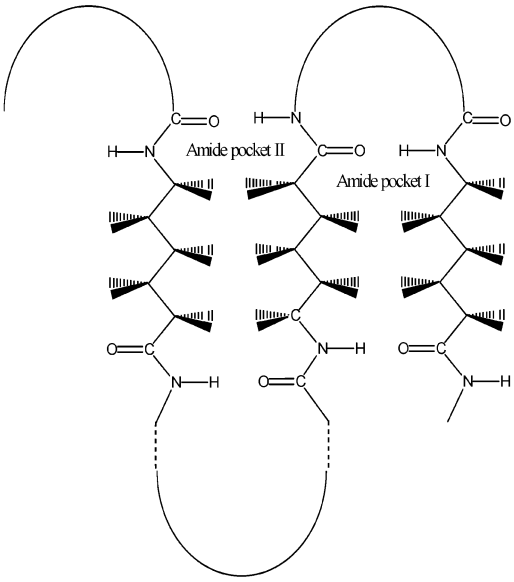

Figure 20. Amide pockets for the loop in adjacent sheet.

One factor comes from the loop parts (see Figure 19). The loop parts need more space than the straight stem segment. Thus, there exists a strong repulsion energy of the loop parts for zero sheet displacement of *eclipse fold-sheet stacking*, as shown in Figure 19a. In addition, the amide part provides much space for the loop of the adjacent sheet, as shown in Figure 16b.

The second factor is that the stacking between the stem parts is better than the stacking between the loop part and the stem part, which is not significant compared with the first factor.

For *eclipse fold-sheet stacking*, the best place to accommodate the adjacent loop is the *amide pocket I* as shown in Figure 20. Thus, the best fold-sheet displacement is $^3/_{14}b$.

For *staggered fold-sheet stacking*, there is no strong repulsion energy between adjacent loop parts for zero sheet displacement. Here the best place to accommodate the adjacent loop is *amide pocket II* instead of *amide pocket I*, as shown in Figure 20. Thus, the best fold-

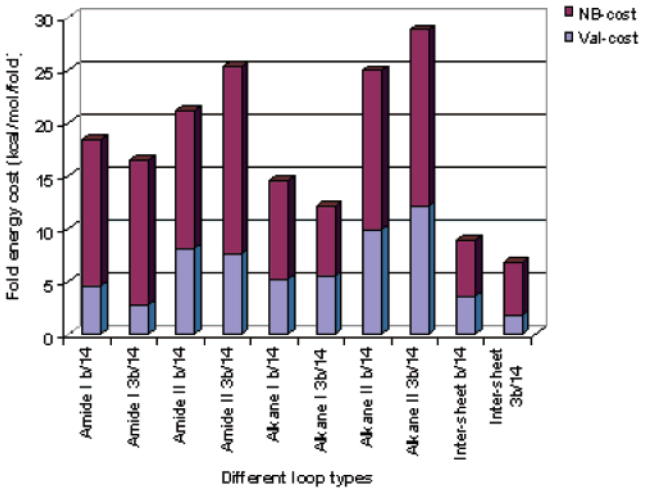

Figure 21. Fold energy cost of different types of loops for 3D lamella crystal.

sheet displacement is $^{2}/_{14}b$. See Figure 18 for the energy comparisons.

These results of the optimum sheet displacement are consistent with the conclusion from fiber X-ray results.[6]

4.5. Optimum Loop Type in 3D Lamella Crystal. Section 4.3 found that the optimum loop type for an individual molecule is *alkane loop type I*. In the 3D lamella crystal, this might change because of *inter-H-bonds* (including H-bonds formed between adjacent loops) and different ways of stacking of the folded layers.

To simplify the comparisons, we consider only *eclipse fold-sheet stacking* and *loop stacking type I* in constructing 3D lamella crystals of all five different loop types.

For *intrasheet loop type*, the 3D lamella crystal structures were constructed from EAP infinite chain model structures.

For *intersheet loop type*, the lamella crystal structures were constructed from EAA infinite chain model structures.

For the fold sheet displacement, we considered only $^{3}/_{14}b$ and $^{1}/_{14}b$.

The results in Figure 21 show that, in the 3D lamella crystal structure, the *intersheet* loop between H-bond sheets is more stable by 5.3 (kcal/mol)/fold than the best *intrasheet* loop (*alkane loop type I*). The reason for this is the lack of loop ring constraints for the fold *between* H-bond sheets, allowing greatly reduced strain and allowing 100% of the H-bonds to be formed.

The *intersheet* loop leads to *inter-H-bonds*, which considering the dynamics of the crystal growth should be worse than loops with *intra-H-bonds* (see section 3.4).

The four types of loops with *intra-H-bonds* have relative energies in the 3D lamella crystal in the same order as for individual molecules. Thus, from best to the worst, they are as follows: *alkane loop type I*, *amide loop type I*, *amide loop type II*, and *alkane loop type II*. Although the amide groups in the *amide loop type I* can form weak H-bonds between adjacent loops, this costs a significant amount of packing energy (involving the methylene group and the amide group from stem to loop). The result is that *alkane loop type I* remains the best type for *intrasheet* loops.

Thus, *alkane loop type I* should be the dominant loop type for 3D lamella crystals of nylon 6. However, it is not possible to have *alkane loop type I* in both sides of the stem if there are an odd number of amide units in the straight stem segment. On the other hand *amide loop type I*, which is only 4 (kcal/mol)/fold worse than *alkane loop type I*, is allowed no matter how many amide units are in the straight stem segment. Thus, we expect that the lamella in experimental structures will have coexisting *alkane loop type I* and *amide loop type I*, but with a majority of *alkane loop type I*.

4.6. Monoclinic vs Triclinic. All the folded crystal structures above are monoclinic unit cells (Figure 22a) in which alternate sheet displacements are EAP+3 and EAP−3. In Figure 22b, we consider the best lamella structure of nylon 6 when each sheet displacement is the same (EAP+3), leading to a triclinic unit cell. We find that triclinic is 0.213 (kcal/mol)/residue more stable than monoclinic. This is explained by our amide pocket model. The amide pocket effect is not quite as good if the same pocket must provide space for both adjacent loop parts as in Figure 22a. The monoclinic and triclinic lamella in Figure 22, parts a and b, are the extreme case of perfectly ordered structures. More likely is that growth kinetics will lead to lamella illustrated in Figure 22c, which has a nearly random combination of Figure 22, parts a and b. The lamella in Figure 22c would be entropically favored and is probably close to the real lamella for nylon 6.

From fiber X-ray,[6] it has been determined that the lamella in the nylon 66 α form is progressive shear (Figure 22b) whereas the nylon 6 α form and the nylon 66 β form have staggered shear (Figure 22a). This difference between nylon 66 and nylon 6 arises because it is easier for the amine residue in nylon 66 to form the loop (due to less loop constraint than in the carbonic acid residue). Also, the amine residue of nylon 66 is bigger than the residue of nylon 6. Thus, the amide pocket effect in nylon 66 should be more significant than in nylon 6, leading to a stronger preference for progressive shear observed in nylon 66 α.

A progressive shear was also concluded to be favored for nylon 46[39] and explained it from surface H-bonds with an assumption that the fold part including two amide units.[39] Our amide pocket model explains the enthalpy favorable progressive shear without such an assumption. Further work needs to be performed for nylon 66 and nylon 46 to clarify the best loop structure and competing factors.

5. Summary

Using the MSXX force field (derived from ab initio quantum calculations), we predict the crystal structures and folded (lamella) structures of nylon 6.

(1) Assuming infinite chains and evaluating the free energy for all 112 regular crystal structures, we find three classes of regular crystal structures: α form (with amide bonds parallel to the methylene sheets), γ form (with amide bonds ∼ perpendicular to the methylene sheets), and δ form (somewhat intermediate between α and γ). These results for α and γ agree well with experimental data. We find that at 300 K the α form is most stable with γ and δ higher by 0.4 and 0.3 kcal/mol (per amide), respectively. The Young's modulus in the chain direction is 295 GPa for α, 135 GPa for γ, and 253 GPa for δ. The only experimental data is 168 GPa for α which is below the calculated value because of the finite thickness of the lamella, the disorder of the chain conformation, and nonperfect crystal in the experimental system.

(2) The concepts of *molecule*, *intra-H-bonds*, and *inter-H-bonds* are introduced, and we find the thermostability

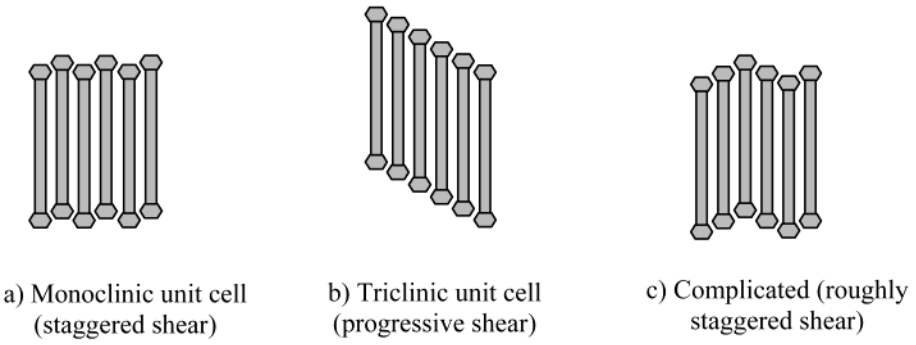

Figure 22. Various stacking schemes of H-bonded sheets.

of α form over other forms comes from *intra-H-bonds* in α form, which are dynamically and entropically favored.

(3) Five detailed transition steps between α form and γ form are proposed and the structures of the two metastable crystalline β forms and the δ form are identified. The structure of the β form, (which has disordered chain conformations and H-bonds in [100], [010], and [1$\bar{1}$0] directions) is consistent with the fiber X-ray results from Auriemma et al.[24] The δ form defined here accounts for the metastable crystalline phase between the β form and the γ form and fits the characteristics of the metastable crystalline discussed by Murthy.[23] It has a similar fiber-axis diffraction scan as the α form and has a similar equatorial diffraction scan as the γ form. These results suggest that stretching and relaxing the fibers would transform between γ and δ.

(4) The H-bond schemes for all regular crystal structures are examined. We find that the γ form has a more linear H-bond than the α form, which is consistent with the conclusion from solid NMR[1].

(5) Since nylon forms lamellae with finite thickness in the chain direction, we considered all five possible loop structures and the two best (of eight) possible stacking schemes for folded sheets together with 14-folded-sheet displacements. The five types of loop structures of nylon 6 are as follows:

•Two with *intra-H-bonds* including two amide units (called *amide loop type I* and *II*).

•Two with *intra-H-bonds* including one amide unit (called *alkane loop type I* and *II*).

•One with *inter-H-bonds* including one amide unit.

We find that for individual molecules the *alkane loop type I* is the best with the others worse by at least 4.5 (kcal/mol)/fold. However in 3D lamella crystals, the inter-sheet case with loops *between* hydrogen bond sheets (leading to γ form or δ form packing) has an energy 5.3 (kcal/mol)/fold lower than the best intrasheet case. This is because there is no ring constraint on the structure of the loops.

We find that the optimum lamella for α form have the alkane loop fold (one amide per loop) and pack so that adjacent sheets are displaced by ± 3.7 Å ($^3/_{14}b$), which is in good agreement with the conclusion from fiber X-ray (Holmes[6]). The amide pocket model is proposed to explain the observed sheet displacement in nylon 6, and it can also explain the observed sheet displacement in nylon 66 and progressive shear in nylon 66 and nylon 46.

Acknowledgment. We thank Dr. Siddharth Dasgupta for helpful advice in initiating this project. This research was partially supported by grants from NSF (CHE99-85574), DOE ASCI ASAP, and ARO-MURI. The facilities of the MSC are also supported by grants from DOE, NSF (CHE 99-77872), ARO (MURI), ARO (DURIP), NIH, ChevronTexaco, 3M, Seiko-Epson, Avery-Dennison, General Motors, Kellogg's, Asahi Chemical, Beckman Institute, and Nippon Steel.

References and Notes

(1) Hatfield, G. R.; Glans, J. H.; Hammond, W. B. *Macromolecules* **1990**, *23*, 1654.
(2) Murthy, N. S.; Khanna, Y. P. *Chem. Mater.* **1993**, *5*, 672.
(3) Dasgupta, S.; Hammond, W. B.; Goddard, W. A. III. *J. Am. Chem. Soc.* **1996**, *118*, 12291.
(4) Karasawa, N.; Goddard, W. A., III. *J. Phys. Chem.* **1989**, *93*, 7320.
(5) Dasgupta, S.; Brameld, K. A.; Fan, C.-F.; Goddard, W. A., III. *Spectrochim. Acta, Part A 1997*, *53*, 1347.
(6) Holmes, D. R.; Bunn, C. W.; Smith, D. J. *J. Polym. Sci.* **1955**, *17*, 159.
(7) Karasawa, N.; Dasgupta, S.; Goddard, W. A., III. *J. Phys. Chem.* **1991**, *95*, 2261.
(8) Karasawa, N.; Goddard, W. A., III. *Macromolecules* **1992**, 25, 7268.
(9) Arimoto, H.; Ishibashi, M.; Hirai, M.; Chatani, Y. *J. Polym. Sci. A* **1965**, *3*, 317.
(10) Abu Isa, I. *J. Polym. Sci., Polym. Chem. Edn.* **1971**, *9*, 199.
(11) Murthy, N. S.; Szollosi, A. B.; Sibilia, J. P.; Krimm, S. *J. Polym. Sci., Polym. Phys. Edn.* **1985**, *23*, 2369.
(12) Miyasaka, K.; Makishima, K. *J. Polym. Sci. A1* **1967**, *5*, 3017.
(13) Miyasaka, K.; Ishikawa, J. *J. Polym. Sci. A2* **1968**, *6*, 1317.
(14) Hiramatsu, N.; Hirakawa, S. *Polym. J.* **1982**, *14*, 165.
(15) Ziabicki, A. *Collect. Czech. Chem. Commun.* **1957**, *22*, 64.
(16) Ziabicki, A. *Kolloid Z* **1959**, *167*, 132.
(17) Ziabicki, A.; Kedzierska, K. *J. Polym. Sci.* **1959**, *2*, 14.
(18) Avramova, N.; Fakirov, S. *Polym. Commun.* **1984**, *25*, 27.
(19) Roldan, L. G.; Kaufman, H. S. *Polym. Lett.* **1963**, *1*, 603.
(20) Illers, K. H.; Haberkorn, H.; Simak, P. *Makromol. Chem.* **1972**, *158*, 285.
(21) Stepaniak, R. F.; Garton, A.; Carlsson, D. J.; Wiles, D. M. *J. Polym. Sci., Polym. Phys. Ed.* **1979**, *17*, 987.
(22) Startsev, O. V.; Iordanskii, A. L.; Zaikov, G. Ye. *Polym. Sci., USSR* **1988**, *30*, 1625.
(23) Murthy, N. S. *Polym. Commun.* **1991**, *32*, 301.
(24) Auriemma, F.; Petraccone, V.; Parravicini, L.; Corradini, P. *Macromolecules* **1997**, *30*, 7554.
(25) Malta, V.; Cojazzi, G.; Fichera, A.; Ajo, D.; Zanetti, R. *Eur. Polym. J.* **1979**, *15*, 765.
(26) Salem, D. R.; Weigmann, H.-D. *Polym. Commun.* **1989**, *30*, 336.
(27) Murthy, N. S.; Minor, H. *Polym. Commun.* **1991**, *32*, 297.
(28) The energy difference between $P1$ and $P2_1$ is negligible. We find that $P2_1$ keeps the same shape for the two amide units in each chain in the simulated unit cell while $P1$ does not. Thus we considered only $P2_1$.
(29) Simon, P.; Argay, Gy. *J. Polym. Sci., Polym. Phys. Ed.* **1978**, *16*, 935.
(30) Leon, S.; Aleman, C.; Munoz-Guerra, S. *Macromolecules* **2000**, *33*, 5754.
(31) Sakurada, I.; Kaji, K. *J. Polym. Sci. C* **1970**, *31*, 57.
(32) Welch, P.; Muthukumar, M. *Phys. Rev. Lett.* **2001**, *87*, 21, Art. No. 218302.

(33) Arimoto, H. *J. Polym. Sci. A* **1964**, *2*, 2283.
(34) Murthy, N. S.; Szollosi, A. B.; Sibillia, J. P.; Krimm, S. *J. Polym. Sci., Polym. Phys. Ed.* **1985**, *23*, 2369.
(35) Zhao, Y. L.; Wu Y. D. *J. Am. Chem. Soc.* **2002** *124*, 1571.
(36) Hoffman, J. D. *SPE Trans.* **1964**, 315.
(37) Jones, N. A.; Sikorski, P.; Atkins, E. D. T.; Hill, M. J. *Macromolecules* **2000**, *33*, 4146.
(38) Trifan, D. S.; Terenzi, J. F. *J. Polym. Sci.* **1958**, *28*, 443.
(39) Bermudez, M.; Leon, S.; Aleman, C.; Munoz-Guerra, S. *J. Polym. Sci. Polym. Phys. Edn.* **2000**, *38*, 41.

MA020815N